IET Microwaves, Antennas & Propagation

Research Article

IET Journals
The Institution of Engineering and Technology

One-dimensional leaky-wave antenna with scanning through the broadside based on sinusoidally modulated reactance surface

ISSN 1751-8725
Received on 14th January 2018
Revised 27th September 2018
Accepted on 17th October 2018
E-First on 12th December 2018
doi: 10.1049/iet-map.2018.5497
www.ietdl.org

Nasser Montaseri[1], Alireza Mallahzadeh[1] ✉

[1]*Department of Electrical and Electronic Engineering, Faculty of Engineering, Shahed University, Tehran, Iran*

✉ *E-mail: mallahzadeh@shahed.ac.ir*

Abstract: A dispersion diagram (DD) and radiation property in a wide-band frequency range are considered for a periodic leaky-wave antenna (PLWA) based on artificial reactance surface (ARS). In the first step, the surface impedance versus gap spacing over a wide frequency band is obtained using full-wave simulation results. In the second step, the frequency dependency effect of ARS on DD of PLWA in the special frequency band is theoretically analysed. The new DD provides a simple way to analyse the radiation beam angle in a wide frequency band for these types of periodic structures. To mitigate and almost eliminate the open stopband, special parameters of sinusoidally modulated ARS are theoretically analysed and the results show how to achieve minimum variations in attenuation near the broadside. By nearly eliminating the open stopband's behaviour, the proposed antenna is able to scan through the broadside without any rapidly varying attenuation. Simulation and measurement results of the proposed antenna validate the theoretical analysis.

1 Introduction

Recently, periodic leaky-wave antennas (PLWAs) have received considerable attention, especially with respect to their millimetre wave applications. These antennas have a low-profile construction, structural simplicity for fabrication, and can easily produce highly directive beams [1]. Owing to their periodicity, the Floquet's theorem is used to analyse these structures [2]. In PLWA with period p along the x axis, the wavenumber consists of an infinite number of space harmonics (Floquet harmonics), with wavenumbers $k_{x_n} = \beta_n - \mathrm{j}\alpha$, where $\beta_n = \beta_0 + 2n\pi/p$ (n is an integer). The fundamental space harmonic with wavenumber $k_{x_0} = \beta_0 - \mathrm{j}\alpha$ which carries most of the power is usually a slow wave ($\beta_0 > k_0$, where k_0 is the wavenumber in free space). Therefore, leakage will occur from the fast space harmonic (the $n = -1$ space harmonic is usually the one that is radiated with $-k_0 < \beta_{-1} < k_0$). It should be noted that the radiated beam angle can be aimed from backward ($-k_0 < \beta_{-1} < 0$) to forward ($0 < \beta_{-1} < k_0$) quadrants as the frequency increases.

In these antennas, it is very difficult to obtain a beam radiating exactly at the broadside because the open stopband occurs around the broadside. At the open stopband region, the attenuation constant varies rapidly and the input match to the antenna typically becomes quite poor. An initial method to reduce the open stopband bandwidth (BW) is to introduce two elements per unit cell [3, 4]. This technique cannot completely eliminate but significantly mitigates the open stopband BW. Later, several methods for the open stopband suppression of PLWAs have been proposed by utilising a reflection cancellation [5], impedance matching of unit cells [5, 6], and implementing asymmetric unit cells [7, 8].

In recent years, a new topology of planar PLWAs has been proposed based on modulated metasurfaces [9, 10]. In these planar antennas, the extreme controls of electromagnetic waves can be obtained using metasurfaces. Metasurfaces can be realised by periodic small elements printed on a ground slab with or without a shorting via [11, 12]. In the first step, the Sievenpiper group [9] presents both linearly and circularly polarised PLWAs based on isotropic and anisotropic impedance surfaces, respectively. Later, in [10], a circularly polarised PLWA is designed based on the modulated isotropic reactance surface. Then, circularly polarised antennas based on the planar anisotropic metasurfaces are designed for space applications [13, 14]. An increasing amount of research has recently been conducted on antennas for designing multi-beam radiations. For the first time, authors in [15] present an efficient method based on concepts of holographic and PLWAs to realise the double-beam radiation. Afterwards, analysis and design of a multi-beam antenna based on anisotropic metasurfaces are considered in [16].

In one-dimensional (1D) periodicity, Oliner and Hessel [17] theoretically described electromagnetic propagation and field distribution along a sinusoidally modulated reactance surface (SMRS) as a method to increase the gain of surface wave antennas. Patel and Grbic [18] expanded this idea as a way to design a printed PLWA. Furthermore, they properly described the step-by-step design procedure for designing a 1D PLWA with the desired beam angle at a single frequency. More recently, researchers have also designed practical PLWAs utilising sinusoidally modulated structures, which operate in the microwave [19–21] as well as in the THz frequencies [22]. Similar to metamaterials, metasurfaces are dependent on frequency. Consequently, the parameters of modulated metasurfaces in PLWA depend on frequency changes. In the method described by Patel and Grbic [18], the parameters of sinusoidally modulated artificial reactance surface (ARS) and, therefore, the radiation beam angle are considered only at a design frequency.

In this study, we have theoretically described the broadband performance of ARS and its effect on the dispersion diagram (DD). Furthermore, both phase and attenuation constants are theoretically calculated for SMRS. In order to mitigate the open stopband effect and achieve broadside radiation, the reduction in the rapidly varying attenuation constant is investigated near the broadside. The DD related to the parameters of ARS is obtained to directly determine the radiation beam angle in a wide frequency band. Finally, to verify the theoretical calculations, the radiation properties of the simulated and measured antenna are compared.

2 Realisation of reactance surface

The ratio of electric to magnetic fields near a surface is defined as the surface impedance. For example, the perfect electric conducting (PEC) and perfect magnetic conducting (PMC) surfaces are zero- and high-impedance surfaces, respectively. Recently, some types of periodic structures have been introduced, including a square patch printed on a grounded slab and pins on a ground plane. From a macroscopic viewpoint, these structures can be

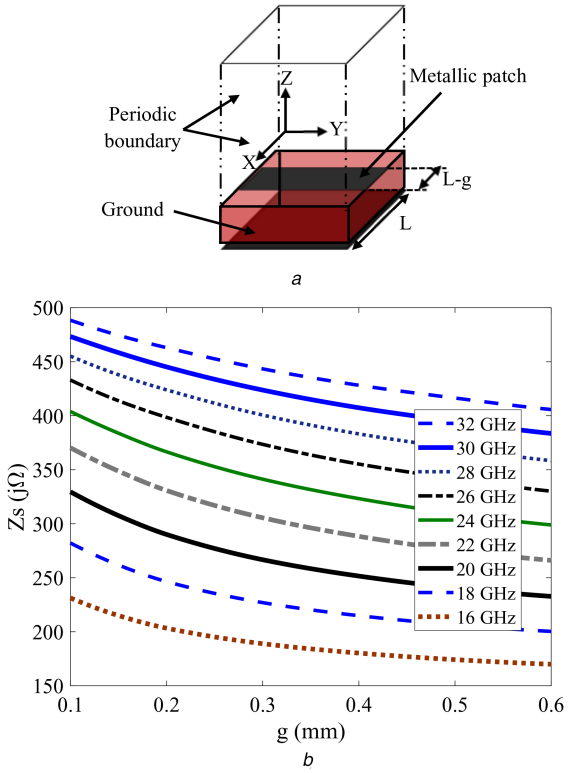

Fig. 1 *Artificial reactance surface*
(a) Three-dimensional view of the unit cell used for the scalar impedance surface, ***(b)*** Surface impedance versus gap spacing at several frequencies

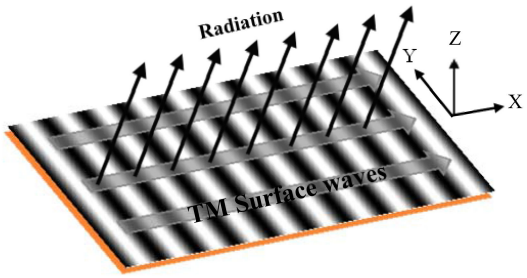

Fig. 2 *Field distribution of TM surface wave is gradually leaked into free space and the radiation phenomenon occurs*

described as effective impedance surfaces. Hence, researchers refer to them as metasurfaces [13] or artificial impedance surfaces [9].

In [2], it is shown that the reactance and capacitance surfaces can support TM and TE surface wave modes, respectively. In this study, we designed a 1D artificial impedance surface by forming a *quasi*-periodic metallic patch printed on a grounded dielectric substrate. The proposed unit cell of scalar impedance surface is shown in Fig. 1*a*, consisting of periodic boundary condition to the four vertical walls. The unit cell is based on *Rogers 4003* substrate ($\epsilon_r = 3.55$, $\tan\delta = 0.0027$) with a thickness of $h = 1.524$ mm and periodic constant of $L = 1$ mm.

To calculate the effective surface impedance, the single unit cell is simulated using the high-frequency structure simulator (HFSS) in eigenmode method [9]. In this method, the main purpose is calculating the phase difference ϕ across the unit cell along the x-axis. The results show that the phase difference obviously depends on a gap size and even frequency. On the other hand, assuming the constant g, the frequency alteration causes variations in ϕ, resulting changes in the surface impedance. In fact, the surface impedance depends on both frequency and gap size for the special unit cell. Hence, the relation between the phase difference and surface impedance can be corrected by the following equation

$$Z_s(k_0, g) = \mathrm{j}\eta_0\sqrt{\left(\frac{\phi(k_0, g)}{k_0 L}\right)^2 - 1}, \tag{1}$$

where η_0 is the impedance in free space. The numerical results given by the eigenmode method are shown in Fig. 1*b* in various frequencies. Moreover, the surface impedance depends on other parameters such as a period constant, a dielectric constant substrate, and the substrate thickness. The impedance value can be increased as L, ϵ_r, or h increases [9].

3 Surface wave interaction with an SMRS

The propagation of TM surface wave on the SMRS has initially been studied by Oliner and Hessel [17]. Surface impedance is defined as the following expression

$$Z_{surf} = \mathrm{j}\eta_0 X'\left[1 + M\cos\left(\frac{2\pi x}{p}\right)\right], \tag{2}$$

where x corresponds to the direction of surface wave propagation along the reactance surface, and p is the period. Owing to the periodicity of the reactance surface, the fields above the surface can be expanded in infinite numbers of space harmonics. When the reactance surface is excited by the TM mode of surface wave, the leakage phenomenon occurs from the fast space harmonics. Fig. 2 illustrates the direction of this radiation from the SMRS where the light and dark areas correspond to high and low reactance values, respectively.

In the SMRS, one period (p) of the reactance surface can be realised using a discrete array of ARS. The impedance value at each segment can be properly realised by ARS with an appropriate gap size. In this kind of PLWAs, the $n = -1$ space harmonic is usually used to radiate into free space [17]. Therefore, the period of the modulated reactance surface for arbitrary radiation angle (θ_{-1}) is approximated as [1]

$$p \simeq \frac{\lambda_0}{\sqrt{1 + X'^2} - \sin(\theta_{-1})}, \tag{3}$$

where λ_0 is the wavelength in free space. In this study, we show a practical example of the designed PLWA, starting from an SMRS with $X' = 0.75$ and $M = 0.15$ at 20 GHz near the broadside. For example, to achieve a radiation beam angle of about $-6.5°$ at $F_0 = 20$ GHz, (3) yields $p = 11$ mm.

A unit cell, corresponding to one period of the SMRS, is shown in Fig. 3*a*. The gap size between the metallic strips is designed where the ARS has a sinusoidal behaviour with the parameters of $X' = 0.75$ and $M = 0.15$ at the frequency of 20 GHz. Each period of the reactance surface is discretised into 11 segments ($L = 1$ mm) where the minimum and maximum of the gap size (g) are 0.1 and 0.5 mm, respectively. Since a gap size in each segment has a varying effective reactance in the frequency band (Fig. 1*b*), the designed modulated reactance surface is extremely similar to the SMRS with different values of X' and M in other frequencies from a macroscopic viewpoint. These two parameters are determined as follows:

$$X'(F) = \frac{X_{max} + X_{min}}{2\eta_0} \tag{4}$$

$$M(F) = \frac{X_{max}}{\eta_0 X'(F)} - 1, \tag{5}$$

where F is the frequency, and X_{max} and X_{min} are maximum and minimum values of reactance surface as depicted in Fig. 1*b*, respectively. For example, $X' = 0.939$ and $M = 0.128$ are acquired at 24 GHz. In Fig. 3*b*, the normalised average reactance, X', and the modulation factor, M, corresponding to the range of $0.1\ \text{mm} \le g \le 0.5$ mm, are shown in the frequency range of 12–32 GHz. As expected, X' slowly increases as the frequency increases. Furthermore, it is obvious that M has a non-linear behaviour over a wide frequency band.

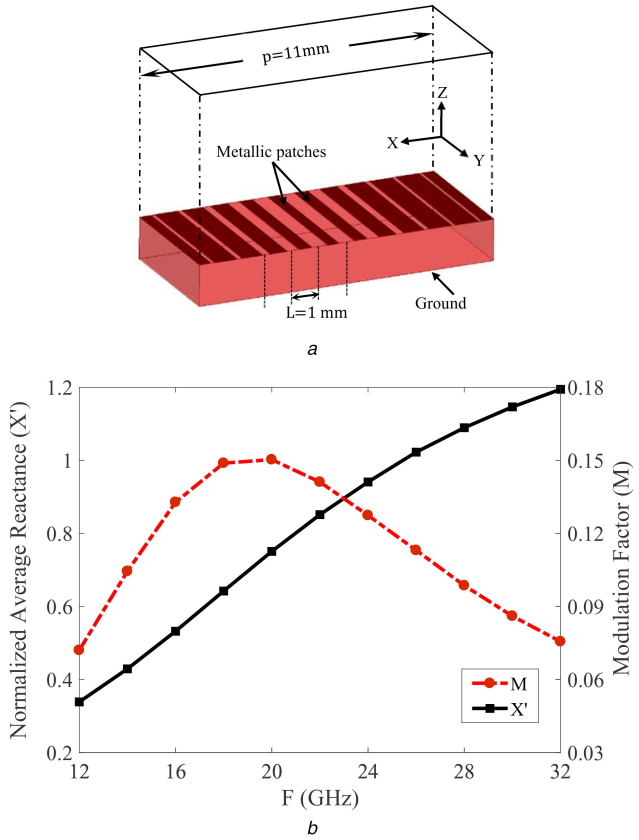

Fig. 3 *Sinusoidally-modulated ARS*

(a) The unit cell corresponding to one period of the sinusoidal reactance surface, ***(b)*** Variation of the normalised average reactance (X') and modulation factor (M) versus frequency (F)

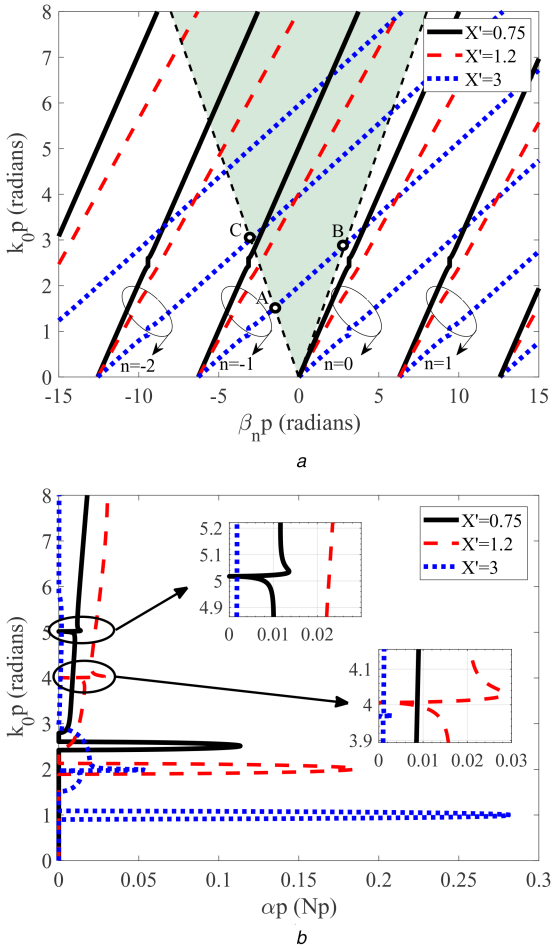

Fig. 4 *Theoretical calculation of guidance characteristics along an ideal SMRS with the fixed $M = 0.2$ and three cases: $X' = 0.75$, 1.2, and 3.*

(a) DD (the shaded region is the radiation region where leakage occurs), ***(b)*** Attenuation constant

3.1 Theoretical consideration of the open stopband

Following the previous study in [17], our study initially considers the phase constants (β_n) which is depicted as DD for several different SMRSs. Afterwards, the attenuation constant (α) is taken into account and its behaviour near the broadside region is exactly considered for this type of structures. According to the analytical formulation described in [17], the fundamental wavenumber ($k_{x_0} = \kappa = \beta_0 - j\alpha$) composing of both phase and attenuation constants is obtained by numerically calculating a continued fraction equation of dispersion relation [i.e. (16) in [17] or (3) in [18]]. Other phase constants of space harmonics (i.e. β_n) can be obtained based on well-known equation $\beta_n = \beta_0 + 2n\pi/p$, where n is an integer. It should be noted that investigating the behaviour of the attenuation constant near broadside region can help to evaluate the open stopband BW [3]. The DD presents the dispersive behaviour of the space harmonic as a plot of k_0p versus β_np, where β_n is the phase constant of any space harmonics. In Fig. 4*a*, the DDs for the case of $M = 0.2$ are presented for three values of $X' = 0.75$, 1.2, and 3. As expected, the fundamental harmonics ($n = 0$) can never be entered into the radiation region (shaded region) and is always bounded to the surface. Furthermore, Fig. 4*a* shows that the dispersion curve slope can be reduced by increasing the value of normalised reactance surface. Thus, the overlap of space harmonics is reduced in the radiation region. For the case of $X' = 3$, point A where $k_0p = 1.513$ represents a frequency that the $n = -1$ space harmonic enters to the radiation region and at point B where $k_0p = 2.894$, the $n = -1$ space harmonic exists from the radiation region. Additionally, the $n = -1$ space harmonic has a radiation condition between points A and B. On the other side, point C where $k_0p = 3.014$ represents a frequency that the $n = -2$ space harmonic enters to the radiation region. As a result, it is obvious there is no overlap between the $n = -1$ and $n = -2$ space harmonics in the radiation region. Given accessibility of reactance surface with $X' > 3$, it seems that the frequency beam-scanning with high radiation efficiency is achievable. However, in the following, it is indicated that the frequency beam-scanning for high amount of X' is impossible because of significantly high open stopband effect.

As mentioned before, the attenuation constant is the imaginary part of the fundamental space harmonic (i.e. $\alpha = -\mathrm{Im}\{k_{x_0}\}$). The effect of different values of X', at the fixed value of $M = 0.2$, on the attenuation constant (α) is indicated in Fig. 4*b*. For three cases, the high attenuation constant occurs in a closed stopband region where the tangential wavenumber (i.e. $k_{x_n} = \beta_n - j\alpha$) is complex for all the Floquet harmonics. At the closed stopband region $\beta_np = (2n + 1)\pi$ (where $2.42 < k_0p < 2.6$, $1.89 < k_0p < 2.13$, and $0.9 < k_0p < 1.09$ for three cases of $X' = 0.75$, 1.2, and 3, respectively), the wave is bounded to the surface, cannot be leaked into the free space, and is reflected back to the source. It should be noted that the closed stopband can only occur within a part of the slow wave region [2] (i.e. $k_0p < \pi$). It can be observed in Fig. 4*b* that the value of the attenuation constant in the closed stopband region increases as the normalised average reactance increases. Furthermore, it is observed that a sudden change in α occurs in a very small frequency range near the broadside (where $k_0p \simeq 5.018$, 4, and 1.97 radians for three cases of $X' = 0.75$, 1.2, and 3, respectively), which is usually known as the open stopband. In fact, the open stopband region depends on the variation of α. As the variation in α near the broadside decreases, the open stopband BW is mitigated [3]. Using the normalised BW criterion which is defined in [3], the open stopband BWs for three cases of $X' = 0.75$, 1.2, and 3 approximately equal BW = 1.29, 1.91, and 2.43%, respectively.

The effect of the modulation factor M for the fixed $X' = 0.75$ on α and $n = -1$ space harmonic of phase constant (β_{-1}) is presented

in Fig. 5. As expected, the leakage constant decreases when M decreases. On the other hand, Fig. 5 shows that the large variation in α near the broadside has been reduced for small values of M, although α always has the value of zero exactly at the broadside. Moreover, it is clear that the phase constant tends to vary linearly with the frequency when M decreases. The open stopband BWs for $M = 0.1$, 0.15, 0.2, 0.25, and 0.3 approximately equal BW = 0.25, 0.64, 1.29, 1.91, and 3.11%, respectively. Note that if $M = 0$ for the case of no modulation, α equals zero and, therefore, there is no leakage and the radiation phenomena do not occur.

In general, the variation in α and, consequently, the open stopband BW is decreased or even partly suppressed using a small amount of X' and M. On the other hand, the small value of X' causes two fundamental drawbacks: (i) the realisation of ARS is very difficult or even not feasible, and (ii) the radiation condition of higher-order space harmonics (especially for $n = -2$) is satisfied, resulting in the reduction in radiation efficiency (see Fig. 4*a*). In this study, the practical example of PLWA is described with $X' = 0.75$ and $M = 0.15$ at the frequency of 20 GHz. The main reason for allocating this value to X' is the fact that when the scanning occurs through the broadside, the higher-order space harmonics do not satisfy the radiation condition.

3.2 Frequency dependency effect of ARS on DD

A unit cell, corresponding to one period of the SMRS, has the period constant of $p = 11$ mm. The gap size between the metallic strips is designed where the ARS has a sinusoidal behaviour with the parameters of $X' = 0.75$ and $M = 0.15$ at the frequency of 20 GHz. Each period of the reactance surface is discretised into 11 segments ($L = 1$ mm) where the minimum and maximum of the gap size (g) are 0.1 and 0.5 mm, respectively. As the designed reactance surface depends on the frequency (see Fig. 1*b*), the parameters of X' and M related to (2) have varying values in the frequency band. In Fig. 3*b*, the values of X' and M related to the designed unit cell of reactance surface are presented as a function of frequency. For such a periodic structure, we can rewrite the impedance surface as the following expression

$$Z_{\text{surf}} = \text{j}\eta_0 X'(k_0)\left[1 + M(k_0)\cos\left(\frac{2\pi x}{p}\right)\right]. \tag{6}$$

To calculate the fundamental wavenumber tangential to the surface, the dispersion relation which is defined in [17] can be rewritten in a continued fraction form as (7), where $k_{x_0} = \kappa = \beta_0 - \text{j}\alpha$ corresponds to the fundamental wavenumber. Solving (7) numerically for κ for a special k_0 yields the DD of the periodic structure versus frequency

$$\begin{aligned} 1 - \frac{\text{j}}{X'(k_0)}\sqrt{1 - \left[\frac{\kappa}{k_0}\right]^2} = \\ \left\{\frac{M^2(k_0)/4}{1 - \text{j}/X'(k_0)\sqrt{1 - [\kappa/k_0 + 2\pi(-1)/(k_0 p)]^2}}\right. \\ - \frac{M^2(k_0)/4}{1 - \text{j}/X'(k_0)\sqrt{1 - [\kappa/k_0 + 2\pi(-2)/(k_0 p)]^2}} - \cdots \\ + \frac{M^2(k_0)/4}{1 - \text{j}/X'(k_0)\sqrt{1 - [\kappa/k_0 + 2\pi(1)/(k_0 p)]^2}} \\ \left. - \frac{M^2(k_0)/4}{1 - \text{j}/X'(k_0)\sqrt{1 - [\kappa/k_0 + 2\pi(2)/(k_0 p)]^2}} - \cdots\right\} \end{aligned} \tag{7}$$

In Fig. 6*a*, the DD of $n = 0, -1, -2$ space harmonics (β_0, β_{-1}, β_{-2}) related to the ARS that is modulated in a sinusoidal situation (with period $p = 11$ mm) are presented as curve 1. It should be noted that the values of X' and M for curve 1 are exactly selected as the values obtained from Fig. 3*b* in the frequency range of 16–32 GHz. Furthermore, the DDs of some ideal reactance surfaces that are modulated in a sinusoidal situation are theoretically calculated and observed as curves 2–5. The comparison shows that the DD slope

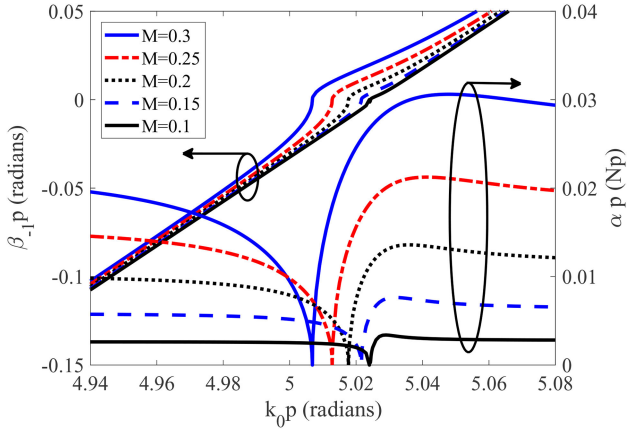

Fig. 5 *Theoretical calculation of the attenuation constant (α) and $n = -1$ space harmonic of phase constant (β_{-1}) versus k_0p for a fixed value of $X' = 0.75$ and five values of $M = 0.1$, 0.15, 0.2, 0.25, and 0.3*

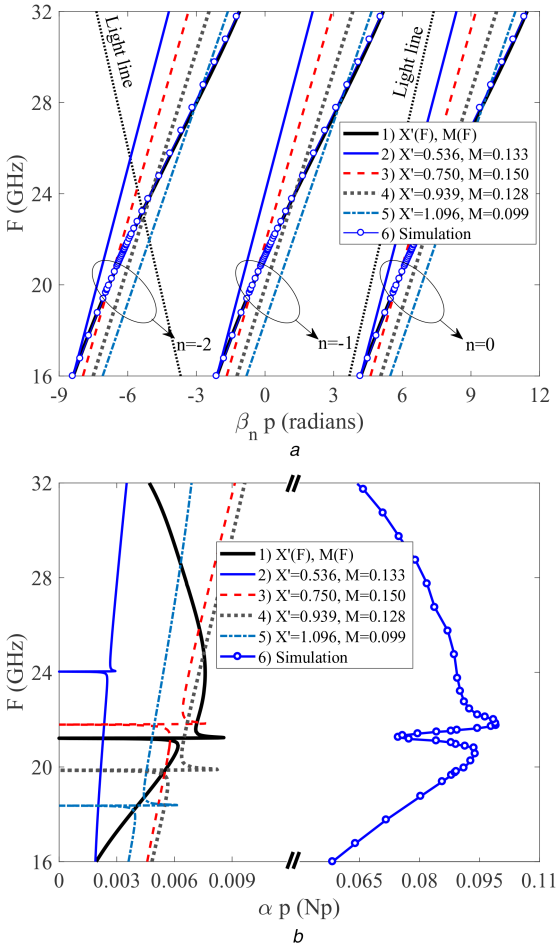

Fig. 6 *Theoretical calculation and HFSS simulation (related to the unit cell in Fig. 3a) of guidance characteristics for several SMRSs*
(a) DD, ***(b)*** Attenuation constant

of the ARS (curve 1) is smaller than the slope of DDs of ideal cases. In fact, the frequency dependency of ARS causes a reduction in the DD slope. Also, the HFSS simulation of the phase constant related to the unit cell shown in Fig. 3*a* is presented as curve 6. Obviously, in Fig. 6*a*, the theoretically calculated phase constant (i.e. curve 1) has a good agreement with the HFSS simulation result (i.e. curve 6). The main advantage of the above discussion is that the radiation beam angle of PLWA may be theoretically calculated for a wide-band frequency range. Besides, behaviours of the attenuation constant are illustrated for six states in Fig. 6*b*. Since in the presented theory, the lossy substrate thickness is ignored and the lossless reactance surface is taken into account,

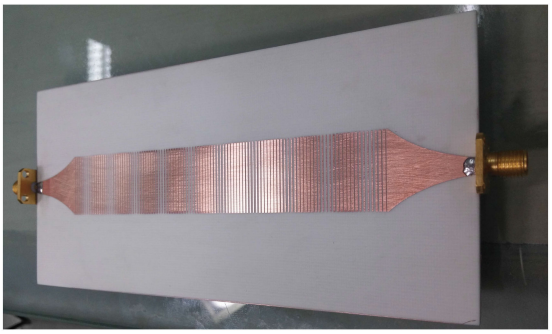

Fig. 7 *Photograph of the fabricated leaky-wave antenna. Both ends of the antenna are tapered to the 50 Ω microstrip transmission line*

values of α obtained by the theoretical calculation are smaller than those achieved by the HFSS simulation [18]. Nevertheless, the theoretical analysis satisfactorily reveals the attenuation constant behaviour, which plays an important role in designing PLWAs, in a wide-band frequency range. The beam angle direction of maximum radiation (θ_{-1}) and half power beam width (HPBW) of the radiation pattern for $n = -1$ space harmonic are easily determined using the following equations [1]

$$\sin(\theta_{-1}) \simeq \frac{\beta_{-1}}{k_0} \tag{8}$$

$$\Delta\theta_{-1} \simeq \frac{1}{(L_A/\lambda_0)\cos(\theta_{-1})} \tag{9}$$

Using (8) and the β_{-1} obtained from curve 1 shown in Fig. 6, the radiation beam of the proposed structure scans from $-34.8°$ to $44.2°$ in the frequency range of 16–32 GHz, respectively. It should be mentioned that the radiation efficiency may be decreased if (i) the higher-order modes of the surface wave become active, (ii) the higher-order modes of space harmonics enter the radiation region, and (iii) the feed form has limitations in illuminating the structure. In the proposed structure, the first higher-order mode of the surface wave, the TE_1 mode, can be propagated at frequencies >30.8 GHz. Moreover, the $n = -2$ of the space harmonic is entered to the radiation region at 23.25 GHz. As the modulation factor in the design antenna has small values, the insignificant amount of power is carried by the $n = -2$ mode in frequencies >23.25 GHz (where $\theta_{-2} = -90°$) in comparison to the $n = -1$ mode. Consequently, its influence on the main beam of the radiation pattern is negligible.

4 Simulation, fabrication, and measurement

Here, to verify the theoretical calculations, the PLWA is considered based on ARS, consisting of ten unit cells. To illuminate the aperture in a uniform manner, the width of the strips is truncated to 20 mm in the fabrication and simulations. In fact, the antenna is fed with a tapered microstrip transmission line with the length of 20 mm and a width varying from 3.5 to 20 mm. To eliminate the reflections from the end of the antenna, the antenna is terminated to 50 Ω load. The fabricated antenna has the dimension of 70×150 mm^2 as shown in Fig. 7. More importantly, to achieve a narrow HPBW in the *H*-plane, the width of strips must be widened proportional to the HPBW. Consequently, the tapered microstrip transmission line is not appropriate for illuminating a wide aperture because higher-order modes of the microstrip transmission line become activate, causing a reduction in the radiation efficiency.

To achieve a high accuracy, a perfect *H*-symmetry boundary condition is used in the full-wave simulation. Therefore, the co-polarisation component of the radiation pattern is merely derived. Simulated (only co-polarisation) and measured (co- and cross-polarisation components) *E*-plane radiation patterns are presented in Fig. 8 at frequencies of 18, 20, 22, and 24 GHz. The discrepancy between simulated and measured patterns is due to fabrication tolerances and probable small defects in measurement process. The

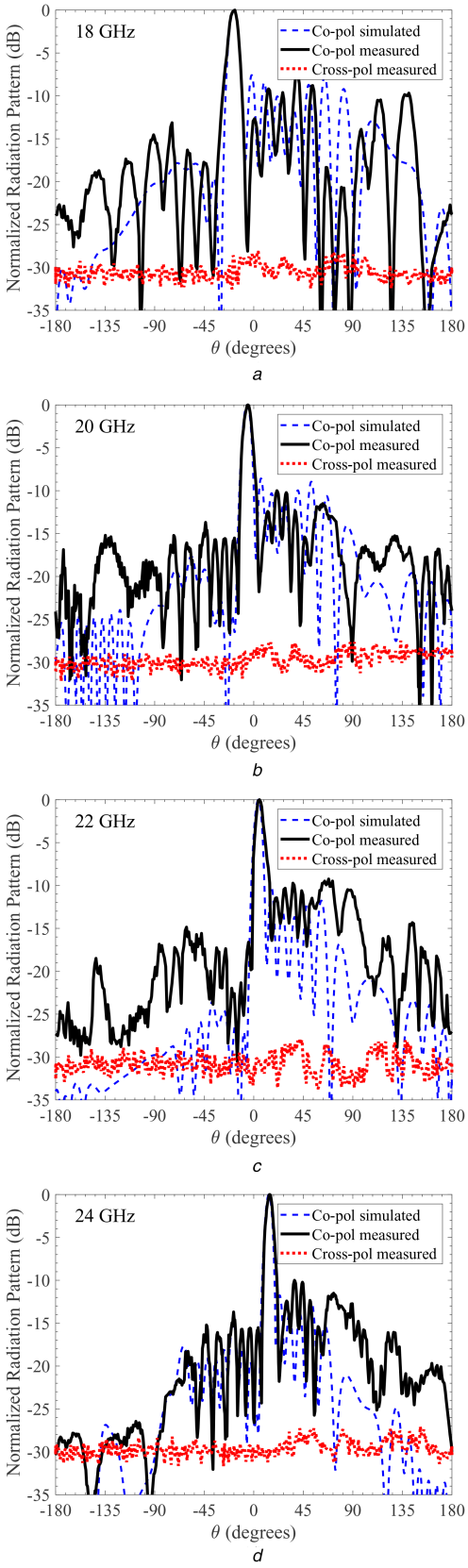

Fig. 8 *Simulated (co-polarisation) and measured (co- and cross-polarisation) E-plane radiation patterns at four different frequencies*
(a) 18, ***(b)*** 20, ***(c)*** 22, ***(d)*** 24 GHz

proposed antenna has a gain of ∼19.7 dB in simulation and 18.8 dB in measurement at the design frequency of 20 GHz. Furthermore, the angles of maximum radiation for the simulated and fabricated antenna are about $-6°$ and $-5.3°$ at 20 GHz, respectively. At this frequency, obtained HPBWs for simulated and fabricated antennas are ∼7.6° and 7.9°, respectively.

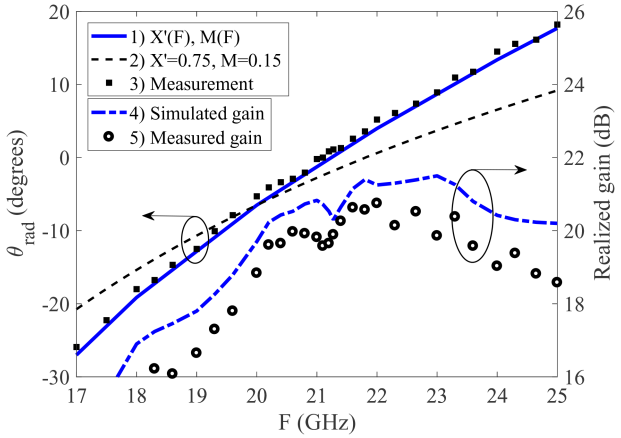

Fig. 9 *Radiation angle and realised gain versus frequency*

Table 1 Comparison of radiation characteristics

Ref. no.	Frequency, GHz	θ_{rad}, °	Cross-pol level, dB	Open stopband width, %	Drop in broadside gain, dB
[18]	[9, 11]	[13, 48]	−22	—	—
[19]	[19, 26]	[−20, 38]	−10	3.5	6
this work	[18, 25]	[−17.1, 18.2]	−28	0.64	0.5

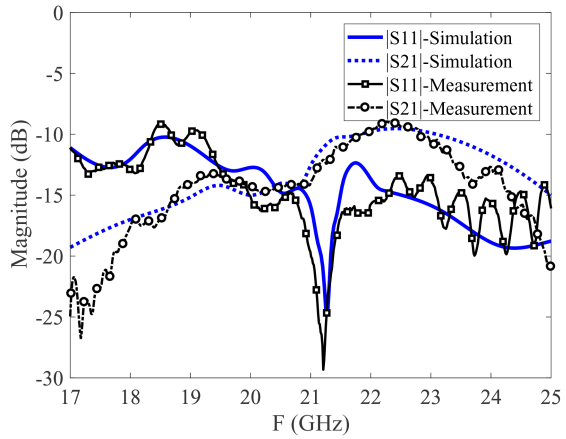

Fig. 10 *Simulated and measured S-parameters versus frequency*

The small deviation between main lobe directions in simulation and measurement results is apparently due to a difference in the dielectric constant in experiment and small errors in the fabrication process. As shown in this figure, the measured cross-polarisation is approximately less than −28 dB over all angles. One significant advantage of the presented antenna is its low cross-polarisation level in comparison to conventional PLWAs [5–8, 19]. Furthermore, the antenna has a simulated radiation efficiency of ∼90% at the design frequency.

In Fig. 9, the obtained radiation angles of the proposed antenna for the three cases below are shown at the wide-band frequency range (i) regarding the frequency dependency effect of ARS, (ii) ignoring the frequency dependency effect of ARS (relying on the method presented in [18]), and (iii) considering the measured direction of the main beam. The beam angles which are calculated by the proposed theory corresponding to curve 1 of Fig. 6 are considerably close to the main beam of the results measured at a wide-band frequency range. This confirms that the presented method can accurately predict the phase constant β and, consequently, the beam angle of the antenna in the frequency band. Comparing curves 1 and 2 of Fig. 9, it is clear that the obtained radiation angle of the supposed ideal SMRS (i.e. curve 2) is accurate only in the design frequency. Moreover, simulated and measured realised gains (curves 4 and 5, respectively) are plotted as a function of frequency in this figure. At the frequency of 21.1 GHz, the radiation beam angle is very close to the broadside and the gain decreases by ∼0.5 dB.

The comparison of radiation characteristics of the proposed antenna and previous sinusoidally modulated structures are shown in Table 1. The open stopband width of the proposed antenna is notably decreased than most of previous works. Therefore, a drop in the gain near the broadside due to the presence of a minor stopband (as shown in Fig. 9) is apparently smaller than that of the previous sinusoidally modulated structure [19]. The measured and simulated scattering parameters are also shown in Fig. 10. In the frequency range of 17–25 GHz, the measured reflection of the fabricated antenna is approximately less than −10 dB. As the fabrication is not accurate enough, and the loss of the connectors is not considered in the simulation, the measured results at frequencies >23 GHz have less disparity than the simulated results. Nevertheless, a good agreement is observed between simulation and measurement results.

5 Conclusion

In this study, an ARS implemented using simple metal strips with a variable gap width over the grounded dielectric substrate is described in a wide-band frequency range. Then, the frequency dependency effect of ARS on DD is theoretically considered for the PLWA based on SMRS, and the new DD is presented for the proposed structure. The main advantage of the new DD is that it allows for the determination of the correct beam angle of maximum radiation in a wide-band frequency range. To achieve a smooth beam-scanning through the broadside, the behaviour of the attenuation constant and, thus, the open stopband BW for the proposed periodic structure is studied. Numerical results illustrate that decreasing the normalised average value of surface reactance, X', and the modulation factor, M, causes a reduction in the variation of attenuation constant, α, and consequently mitigates the open stopband BW. The proposed antenna is simulated and then manufactured. The radiation beam of the fabricated antenna scans from −17.14° to 18.2° in the frequency range of 18 to 25 GHz, respectively. The low level cross-polarisation is another advantage of these types of periodic structures. An excellent agreement is observed among the theoretical calculations, simulation, and measurement results.

6 References

[1] Oliner, A.A., Jackson, D.R.: 'Leaky-wave antennas', in Volakis, J.L. (Ed.): '*Antenna engineering handbook*', (McGraw-Hill, New York, NY, USA, 2007, 4th edn), pp. 11.1–11.56

[2] Hessel, A.: 'General characteristics of traveling-wave antennas', in Collin, R.E., Zucker, F.J. (Eds.): *Antenna Theory*, (McGraw-Hill, New York, NY, 1969), pp. 151–258

[3] Guglielmi, M., Jackson, D.: 'Broadside radiation from periodic leaky-wave antennas', *IEEE Trans. Antennas Propag.*, 1993, **41**, (1), pp. 31–37

[4] Solbach, K., Adelseck, B.: 'Dielectric image line leaky wave antenna for broadside radiation', *Electron. Lett.*, 1983, **19**, (16), pp. 640–641

[5] Paulotto, S., Baccarelli, P., Frezza, F., *et al.*: 'A novel technique for open-stopband suppression in 1-d periodic printed leaky-wave antennas', *IEEE Trans. Antennas Propag.*, 2009, **57**, (7), pp. 1894–1906

[6] Williams, J.T., Baccarelli, P., Paulotto, S., *et al.*: '1-d combline leakywave antenna with the open-stopband suppressed: design considerations and comparisons with measurements', *IEEE Trans. Antennas Propag.*, 2013, **61**, (9), pp. 4484–4492

[7] Otto, S., Al-Bassam, A., Rennings, A., *et al.*: 'Transversal asymmetry in periodic leaky-wave antennas for Bloch impedance and radiation efficiency equalization through broadside', *IEEE Trans. Antennas Propag.*, 2014, **62**, (10), pp. 5037–5054

[8] Otto, S., Chen, Z., Al-Bassam, A., *et al.*: 'Circular polarization of periodic leaky-wave antennas with axial asymmetry: theoretical proof and experimental demonstration', *IEEE Trans. Antennas Propag.*, 2014, **62**, (4), pp. 1817–1829

[9] Fong, B.H., Colburn, J.S., Ottusch, J.J., *et al.*: 'Scalar and tensor holographic artificial impedance surfaces', *IEEE Trans. Antennas Propag.*, 2010, **58**, (10), pp. 3212–3221

[10] Minatti, G., Caminita, F., Casaletti, M., *et al.*: 'Spiral leaky-wave antennas based on modulated surface impedance', *IEEE Trans. Antennas Propag.*, 2011, **59**, (12), pp. 4436–4444

[11] Sievenpiper, D., Zhang, L., Broas, R.F., *et al.*: 'High-impedance electromagnetic surfaces with a forbidden frequency band', *IEEE Trans. Microw. Theory Tech.*, 1999, **47**, (11), pp. 2059–2074

[12] Kildal, P.S., Kishk, A.A., Maci, S.: 'Special issue on artificial magnetic conductors, soft/hard surfaces, and other complex surfaces', *IEEE Trans. Antennas Propag.*, 2005, **53**, (1), pp. 2–7
[13] Minatti, G., Maci, S., De-Vita, P.*, et al.*: 'A circularly-polarized isoflux antenna based on anisotropic metasurface', *IEEE Trans. Antennas Propag.*, 2012, **60**, (11), pp. 4998–5009
[14] Minatti, G., Faenzi, M., Martini, E.*, et al.*: 'Modulated metasurface antennas for space: synthesis, analysis and realizations', *IEEE Trans. Antennas Propag.*, 2015, **63**, (4), pp. 1288–1300
[15] Li, Y.B., Wan, X., Cai, B.G.*, et al.*: 'Frequency-controls of electromagnetic multi-beam scanning by metasurfaces', *Sci. Rep.*, 2014, **4**, p. 6921
[16] González-Ovejero, D., Minatti, G., Chattopadhyay, G.*, et al.*: 'Multibeam by metasurface antennas', *IEEE Trans. Antennas Propag.*, 2017, **65**, (6), pp. 2923–2930
[17] Oliner, A., Hessel, A.: 'Guided waves on sinusoidally-modulated reactance surfaces', *IRE Trans. Antennas Propag.*, 1959, **7**, (5), pp. 201–208
[18] Patel, A.M., Grbic, A.: 'A printed leaky-wave antenna based on a sinusoidally modulated reactance surface', *IEEE Trans. Antennas Propag.*, 2011, **59**, (6), pp. 2087–2096
[19] Podilchak, S.K., Matekovits, L., Freundorfer, A.P.*, et al.*: 'Controlled leaky-wave radiation from a planar configuration of width-modulated microstrip lines', *IEEE Trans. Antennas Propag.*, 2013, **61**, (10), pp. 4957–4972
[20] Panaretos, A.H., Werner, D.H.: 'Spoof plasmon radiation using sinusoidally modulated corrugated reactance surfaces', *Opt. Express*, 2016, **24**, (3), pp. 2443–2456
[21] Ramalingam, S., Balanis, C.A., Birtcher, C.R.*, et al.*: 'Axially modulated cylindrical metasurface leaky-wave antennas', *IEEE Antennas Wirel. Propag. Lett.*, 2018, **17**, (1), pp. 130–133
[22] Esquius Morote, M., Gómez-Díaz, J.S., Perruisseau-Carrier, J.*, et al.*: 'Sinusoidally modulated graphene leaky-wave antenna for electronic beamscanning at Thz', *IEEE Trans. Terahertz Sci. Technol.*, 2014, **4**, (1), pp. 116–122